



# ON THE ROLE OF COHERENT TURBULENT STRUCTURES ON THE NOISE EMITTED BY NON-STRAIGHT TRAILING EDGES

Lourenco Tercio Lima Pereira<sup>1\*</sup>

Francesco Avallone<sup>1,2</sup>

Daniele Ragni<sup>1</sup>

<sup>1</sup> Faculty of Aerospace Engineering, Delft University of Technology, The Netherlands

<sup>2</sup> DIMEAS Department, Politecnico di Torino, Torino, Italy

## ABSTRACT

This work addresses the importance of considering the coherent organization of turbulence structures when predicting the noise from serrated trailing edges. Turbulent flow is the source of broadband trailing-edge noise. The existence of coherence in the turbulent flow departs from the state-of-the-art assumption for noise prediction based on the sum of the different wavenumbers excitations in an incoherent manner. This study addresses whether the latter hypothesis is the underlying cause of the noise underestimation observed from theoretical models for serrated trailing edges at high frequencies. A simplified hairpin model in the form of a bounded vortex filament is used as input to the scattering solution. The vortex filament is used to compute the turbulent velocity and wall-pressure fluctuations induced by the modelled coherent structure. This coherent wall-pressure structure is given as input to a numerical acoustic solver of the diffraction problem, yielding the scattered acoustic field. Results focus on the differences between coherent and incoherent assumptions. It is demonstrated that the acoustic scattering of coherent structures differs from the incoherent sum of the wavenumber spectrum of such structures, showing more consistent results with experimental evidences. The results indicates that modelling of the noise from serrated trailing edges can be improved with a detailed description of the turbulent flow.

**Keywords:** *aeroacoustics, trailing-edge noise, serrated trailing edges*

\*Corresponding author: [l.t.limapereira@tudelft.nl](mailto:l.t.limapereira@tudelft.nl).

**Copyright:** ©2023 Lima Pereira et al. This is an open-access article distributed under the terms of the Creative Commons Attribution 3.0 Unported License, which permits unrestricted use, distribution, and reproduction in any medium, provided the original author and source are credited.

## 1. INTRODUCTION

The prediction of noise generated by the advecting turbulent structures inside a boundary layer near the trailing edge of a wing is based on the solution of the diffraction problem described in [1–4]. This solution is obtained for an advecting gust described as a purely advecting sinusoidal wave excitation, where the streamwise wavenumber is related to the frequency and the gust convective speed ( $k_x = \omega/U_c$ ).

For straight [1] and slanted [5] trailing edges, this procedure results in a dominant cut-on wavenumber-frequency mode, i.e. the one where the wave crests are aligned with the trailing-edge direction. Nevertheless, the noise scattered by more complex geometries, e.g. serrated trailing edges, depends on the contribution of several cut-on modes, as described in [6]. To account for these multiple contributions, the modes are considered uncorrelated from one-another. This assumption yields good comparisons against experimental data available at low frequencies [6, 7] for serrated trailing edges. However, at high frequencies, the methodology often predicts an asymptotic behaviour of the noise reduction. The latter contrasts with experimental [8, 9] and numerical [10, 11] evidences.

In this work, an alternative for the modelled inconsistencies is explored, i.e. the presence of coherent structures inside the turbulent flow. Based on this hypothesis, the coherent interaction of the different wavenumber wall-pressure modes affects the total noise. To account for the presence of coherence, a modelled turbulent coherent structure, in the form of a simplified hairpin, is used as input to a numerical solver of the acoustic scattering diffraction problem. The results are confronted against the incoherent sum of the modes to demonstrate the differences between both assumptions.



## 2. METHODOLOGY

This study requires a representative model for a coherent turbulent structure inside a turbulent boundary layer and a method to predict the acoustic scattering from this incoming structure. The following sections describe, respectively, the coherent structure modelled and the methodology used to assess the acoustic scattering at the trailing edge due to the turbulent structures.

### 2.1 Model of a hairpin coherent structure

The model chosen for the wall-pressure fluctuations induced by a coherent structure is based on an advecting hairpin inside a boundary-layer flow, following the work of [12]. This approach considers a simplified geometry of a finite vortex line to emulate a turbulent hairpin, as illustrated in Figure 1. The geometry of the vortex line is used to predict the velocity and, lately, the wall-pressure fluctuations induced by the hairpin structure. A simplified description of the procedure is provided hereafter. More details can be found in the work of [12].

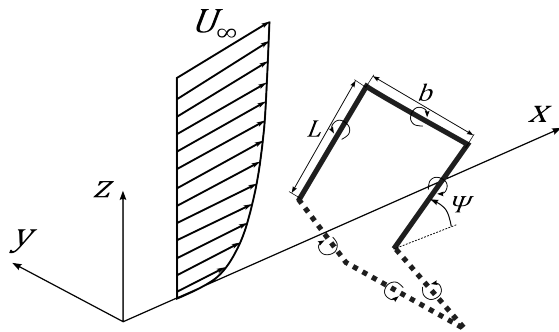


**Figure 1.** Geometric representation of a hairpin vortex line (in grey) on a turbulent boundary layer flow. The dashed lines represent the mirrored hairpin used in the mathematical description of the wall effects.

The model is based on an idealized hairpin structure consisting of two slanted legs of length  $L$  placed at an angle  $\psi$  with respect to the flow, and a straight head of spanwise extent  $b$ . This geometric structure represents a horseshoe vortex of uniform vorticity  $\Gamma$ , and radius  $r_c$ .

The velocity fluctuation induced by the presence of the horseshoe structure is computed from the Bio-Savart integral using the Rankine vortex model and the approximation of slender vortex streaks [12]. The proposed approximation is used to compute the velocity field induced by each of the legs and the hairpin's head.

The fluctuating velocity field is combined with the mean boundary-layer velocity profile to compute the induced wall-pressure fluctuations. For that, the mean boundary-layer velocity profile ( $U$ ) and the wall-normal velocity fluctuation field ( $w$ ) created by the hairpin vortex and its mirrored vortex below the wall are used as input to the solutions of the pressure Poisson equation, obtained from the Green's function formulation for the pressure (eq. 1).

$$p_{\text{wall}}(t, \vec{x}, z=0) = \frac{\rho_o}{2\pi} \int_{-\infty}^{\infty} \int_{-\infty}^{\infty} \int_{-\infty}^{\infty} \frac{1}{\|\mathbf{x} - \mathbf{x}'\|} \frac{\partial U}{\partial z} \frac{\partial w}{\partial x} d\mathbf{x}' \quad (1)$$

The latter integral is computed numerically using a trapezoidal approach. The derivatives are predicted using a second-order finite differences scheme. Figure 2 illustrates the process with the streamlines induced by the presence of a hairpin on a mean uniform flow and the induced wall pressure due to the presence of the hairpin structure.

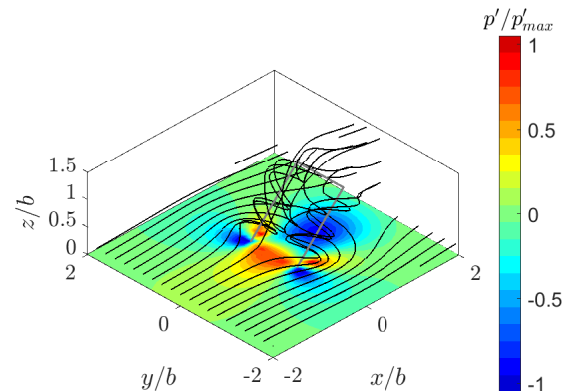


**Figure 2.** Example streamlines induced by the presence of a hairpin in the mean flow and the wall-pressure induced by the hairpin.

#### 2.1.1 Physical quantities

The model discussed requires a description of the mean boundary-layer flow above the wall and a geometrical description of the hairpin structures.

The former is obtained from a Spalding boundary layer model [13] added to the wake model of Coles [14].

The size of the hairpin structures follows [12] and is based on a stochastic distribution of possible hairpin sizes.

**Table 1.** Parameters chosen for the 6 hairpins geometries selected for the study.

$z/\delta$ ( $b/\delta$ )	$L/\delta$ ( $\sqrt{2}b/\delta$ )	$z^+$ ( $b^+$ )	$\psi$ [°]	$r_c/b$
0.10	0.14	40	45	0.05
0.13	0.18	50	45	0.05
0.17	0.25	60	45	0.05
0.23	0.32	80	45	0.05
0.30	0.43	110	45	0.05
0.40	0.57	140	45	0.05

It is assumed that these coherent structures happen at every possible size within the turbulent flow. For each possible hairpin head size ( $b$ ) an occurrence density ( $n_e$ ) is associated. According to [12], the occurrence density is related to the hairpin size following eq. 2.

$$n_e \propto \frac{1}{b^3}. \quad (2)$$

From the distribution of hairpins, the wavenumber spectrum of a single hairpin can be estimated by integrating the wavenumber spectrum of the obtained coherent structures times the occurrence density of all possible hairpin sizes (eq. 3).

$$\phi_{pp}(k_x, k_y) = \int_{b_{\min}}^{b_{\max}} n_e(b) |S_{pp}(k_x, k_y, b)| db. \quad (3)$$

To reduce the computational costs required for the numerical integral, the solution is truncated by considering only 6 possible hairpin sizes (defined by  $b$ ). The low accuracy from the small number of points is avoided by assuming self-similarity and scaling the wall pressure computed for hairpin sizes ( $b$ ) outside the 6 values chosen, i.e. the estimation of eq. 3 uses an scaled value of  $S_{pp}$  for values of  $b$  between the chosen ones.

Table 1 summarizes the 6 possible hairpin sizes selected. Following the literature, all the hairpins have an angle  $\psi$  equivalent to  $45^\circ$ , a leg size of  $L = \sqrt{2}b$ , and a vortex core radius of  $0.05b$  [12].

The boundary layer and geometry of the sawtooth trailing-edge serration chosen for the study are based on the benchmark model presented in the work of [15]. The 2D NACA 63<sub>3</sub>-018 airfoil model is a benchmark airfoil for validating acoustic measurements under different facilities and scales [15]. Table 2 describes the main boundary-layer and serration geometric parameters required for the study.

**Table 2.** Boundary-layer parameters and geometry of the sawtooth trailing-edge serration.

Parameter	Symbol	Value	
Flow speed	$U_\infty$	20	m/s
Boundary layer thickness	$\delta$	10	mm
Friction velocity	$u_\tau$	0.6	m/s
Wake parameter	$\Pi$	2.0	
Serration height	$2h$	20	mm
Serration wavelength	$\lambda$	10	mm

## 2.2 Scattering solver

The scattering at the trailing edge can be modelled by the diffraction problem shown in the work of [2], based on the work of [1]. The solution is based on an infinitely long plate with a trailing-edge geometry described by the function  $g(y)$ . The scattered acoustic waves are to comply with the homogeneous wave equation (eq. 4). To the equation, a Neumann boundary condition is applied in the wall and a Dirichlet one is applied downstream from the trailing edge, following equation 5.

$$\nabla^2 p - \frac{1}{c_o} \left( \frac{\partial}{\partial t} + U_\infty \frac{\partial}{\partial x} \right)^2 p = 0. \quad (4)$$

$$\begin{cases} \frac{\partial p}{\partial y} = 0, & \text{if } x \leq g(y) \\ p = -p_i(t, x, y), & \text{if } x > g(y) \end{cases} \quad (5)$$

### 2.2.1 Numerical method

A numerical solution of the scattered acoustic field is carried out using the solver COMSOL Multiphysics for both a wavenumber input and a coherent input based on an advecting wall-pressure structure past a hairpin. The solver is based on the wave equation with boundary conditions that follow the ones proposed in [2]. The equation is solved on a half C-shaped domain as shown in Figure 3. The trailing edge represents a transition region between the wall boundary and the wake boundary.

The results of the wavenumber excitations with  $k_y = 0$  are shown in Figure 4 for validation purposes. The numerical solutions are compared against predictions from Ayton's model [3] for the same wavenumber and with Howe's model [16] for the sum of all wavenumbers. The comparisons indicate that the numerical simulations agree well with the predicted noise reduction from the theory. Still, discrepancies exist at the highest frequency tested ( $f = 1000$  Hz).

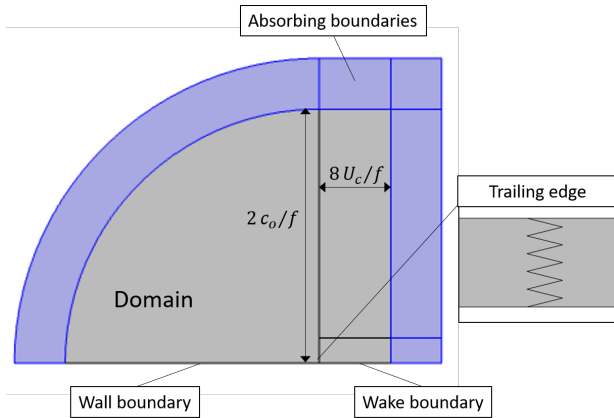


**Figure 3.** Geometry of the centre of the simulation domain used for the software COMSOL. The blue areas represents acoustically absorbing walls.

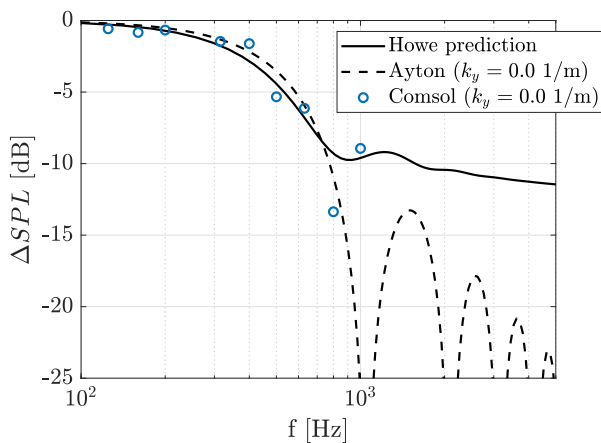


**Figure 4.** Comparison between the numeric and the analytical prediction of the variation of sound pressure level between the serrated and the straight trailing-edge geometry for an incoming wave of  $k_3 = 0$ . The markers show the numerical results. Solid lines represent Howe’s prediction and dashed-lines the results from Ayton’s model [3].

For the coherent structures, a detailed study of the noise also depends on the relative position between the passing coherent structures and the serration location. For that, 3 different spanwise positions of the hairpin centre with respect to the serration location are selected,

namely root, centre, and tip conditions. Figure 5 illustrates these locations with the largest hairpin structure tested ( $bu_\tau/\nu = 140$ ). The numerical results from all the locations are combined with the assumption that the distribution of hairpin locations along the spanwise is uniform.

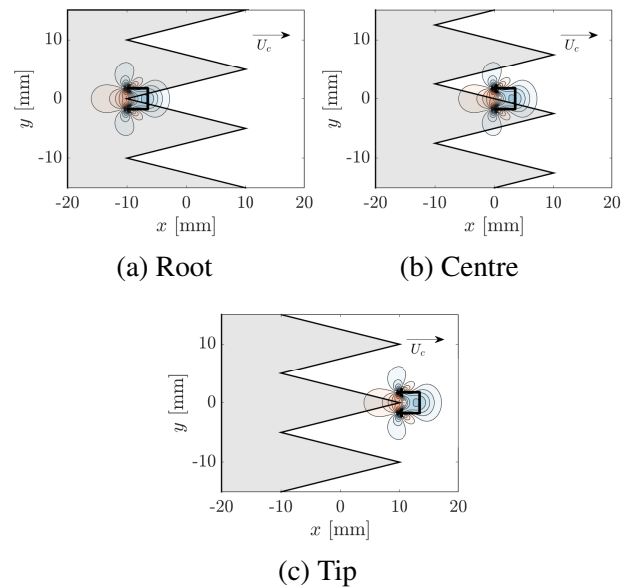


**Figure 5.** Adopted spanwise locations of the hairpin centre with respect to the serrations for the simulations.

### 3. RESULTS

#### 3.1 The wall-pressure fluctuations beneath a hairpin structure

Figure 6 demonstrates the character of the wall pressure excited by the different hairpin structures tested. Downstream from the hairpin, a negative pressure region is created, following the accelerated flow above the hairpin head. Upstream of it, the low-speed streaks are responsible for generating a high-pressure region, as discussed in [17]. The profiles obtained for the different hairpin heights are very similar and appear to have their relative footprint reduced as the hairpin grows larger.

Nevertheless, differences exist in the wall pressure induced on the sides of the hairpin structures. Most notably, aside from the legs of the hairpin, secondary wall-pressure structures are observed. A negative pressure fluctuation

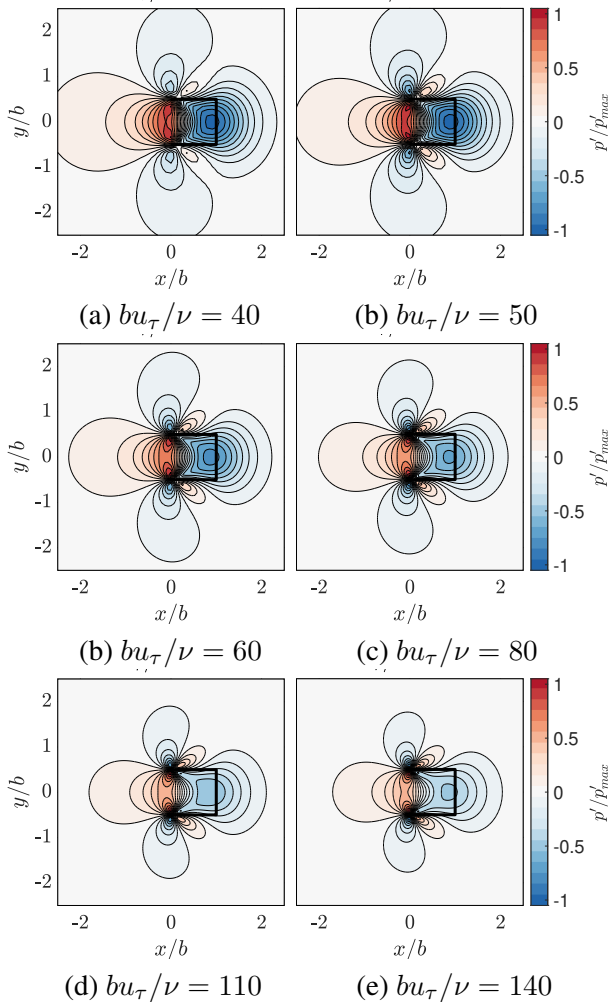


**Figure 6.** Computed wall-pressure fluctuations excited by the different hairpin sizes.

is captured on the side of the hairpin's leg. Just downstream from this low-pressure region, a small region of positive pressure is also seen. The extent of this latter region depends on the height of the hairpin. For the smallest structure tested ( $bu_\tau/b = 40$ ) the positive induced wall pressure is significantly smaller than for the highest one ( $bu_\tau/b = 140$ ).

The importance of these secondary structures lies in the presence of high  $k_y$  wavenumbers, as depicted by the average wavenumber spectrum obtained for each of the coherent structures (Figure 7). For the smallest of the hairpin sizes, the high-level excitation is mostly concen-

trated on the  $k_y = 0$  region. This is in agreement with the measured wavenumber spectrum of the average turbulent flow, as seen in many references [16, 18–20]. However, the larger coherent structures seem to also create a high energy content for  $k_y \neq 0$ , as it can be seen, for example in Figure 7f.

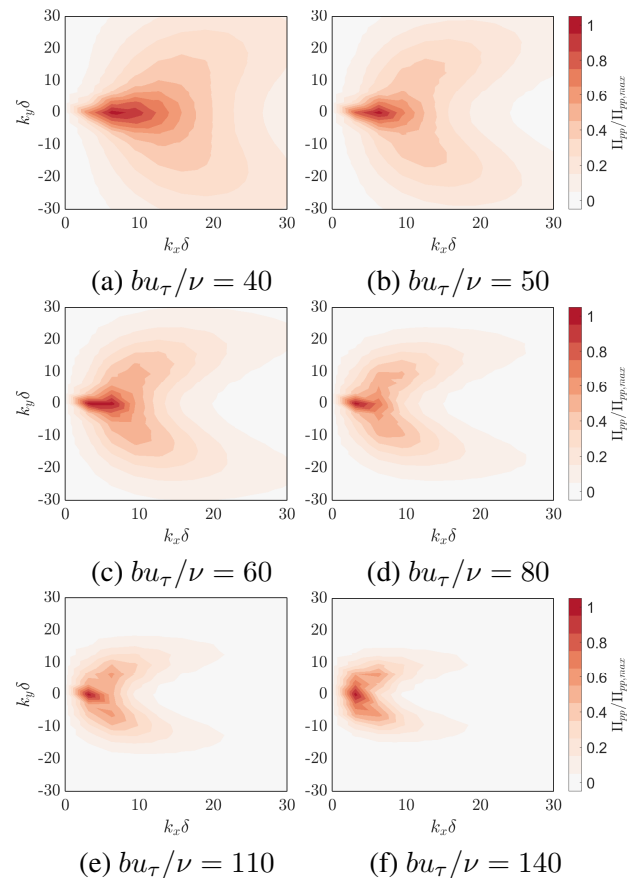


**Figure 7.** Wavenumber spectrum obtained from the wall-pressure fluctuations excited by the different hairpin sizes.

The contribution of each different structure to the average wall-pressure spectrum is shown in Figure 8. From the figure, it is clear that the smallest coherent structures, the ones closer to the wall, are the ones that influence the wall-pressure fluctuations the most. Nevertheless, the larger structures still have a non-negligible contribution, only a few dBs below the smallest hairpins. By summing all the contributions from the different hairpins, the average wall-pressure spectrum can be estimated (shown in black in the figure). It is important to restate here that

the spectrum obtained from the wall-pressure spectrum must be scaled as the absolute intensity of the hairpin vorticity is not defined but rather the relative one with respect to its size. The resulting spectrum shape compares well with the morel of Goody [21] for the wall-pressure spectrum past a turbulent boundary layer under zero-pressure gradient. The figure also shows some of the important trends expected for the wall-pressure spectrum on a zero-pressure gradient turbulent boundary layer, i.e. the scaling with  $\omega^{-0.7}$  at mid frequencies, and with  $\omega^{-5}$  at high frequencies. The agreement indicates the suitability of the methodology and assumptions proposed in [12] for representing the structures governing the wall-pressure fluctuations.

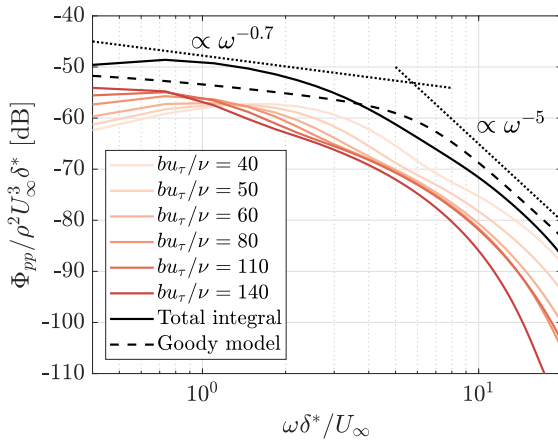


**Figure 8.** Frequency spectrum of the wall-pressure fluctuations excited by different hairpin sizes. The solid black line shows the combination from all hairpin sizes and the dashed-dotted line the predicted spectrum using Goody model [21].

The discussion regarding the energy content of the large structures and the  $k_y \neq 0$  wavenumbers is an important one concerning the noise scattered by serrated trailing edges. This is because the non-straight geometry of the serrations increases the noise scattered for  $k_y \neq 0$  modes while reducing the noise from the  $k_y = 0$  ones. This is the underlying phenomenon behind the noise reduction promoted by non-straight trailing edges as the spectral levels of the turbulent flow are much higher around  $k_y = 0$ .

The findings from Figure 7 indicate that the small-scale structures, the ones with high energy around  $k_y = 0$ , might indeed scatter less noise when passing through a

serrated trailing edge when compared to a straight one. However, the large-scale ones, with high energy around  $k_y \neq 0$ , might have the opposite effect, i.e. they scatter more noise for the serrated trailing edge. This would indicate that the individual contribution of structures of different length scales needs to be evaluated to assess the total noise produced by a serrated trailing edge.

Besides, the wall-pressure structures in Figure 6 emphasize the existence of a phase relationship between the different wavenumbers shown in Figure 7. This means that contributions from different wavenumbers might interact constructively or destructively, differently from the incoherent sum hypothesis commonly assumed.

### 3.2 The scattering properties of a coherent structure

This section is dedicated to the resulting acoustic field scattered by the advecting hairpin structures. Figure 9(a) demonstrates the resulting temporal evolution of the pressure for an observer at  $(x_o, y_o, z_o) = (0, 1, 0)$  meters with respect to the trailing edge. The graph shows the time history of the wall pressure due to the hairpin of size  $bu_\tau/\nu = 140$  for all three spanwise locations along the serrations against the one of the straight trailing edge (black line). Observing from the centre and tip, it is clear the influence of the serrations. The serrated trailing edges make the acoustic field weaker but also more spread in time, which consequently translates to lower noise levels. Interestingly, this is not the case for the structure passing through the root of the serrations. At this location, the teeth align with only the positive or negative fluctuations from the hairpin, which causes the stronger scattering captured (observed in Figure 5a). The resulting noise reduction spectrum from the different hairpin sizes is shown in Figure 9(b) where the position at the centre of the serration is shown. First, it is evident that the noise reduction does not reach the predicted levels from the uncorrelated assumption, indicating a first incompatibility with the hypothesis. As discussed, the scattering of the larger structures produces higher noise levels than the ones of the smaller hairpin structures. Second, the scattering at the centre of the serration is the weakest one, and along the root, noise increase is captured. The overall sum indicates that the noise reduction predicted from the several hairpins is smaller than the one of the incoherent assumptions. Results encourage the idea that the discrepancies between analytical models and measured noise reduction can be also related to the coherent relations within the turbulent boundary layer.

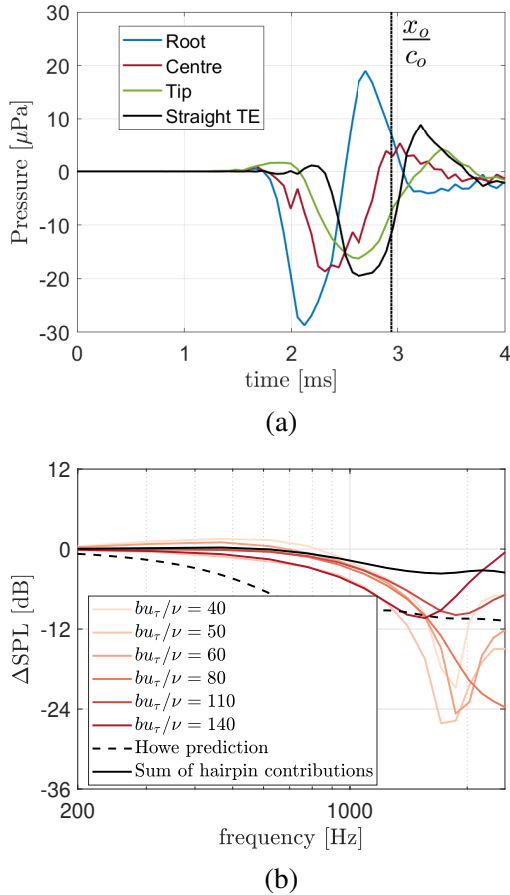


**Figure 9.** Temporal evolution of the wall pressure due to the passing of a hairpin of size  $bu_r/\nu = 140$  at different spanwise locations (a) and noise reduction spectrum of pressure fluctuations from all different hairpin sizes (b). Observer location is set to  $(x_1, x_2, x_3) = (0, 1, 0)$  meters.

#### 4. CONCLUSIONS

This work explores the role of coherent structures on the noise scattered by non-serrated trailing edges. To conduct the study, a hairpin model, based on the work of [12] is selected. 6 different hairpin heights are used and, from those, the wall-pressure fluctuations induced by these coherent structures are estimated. The wall-pressure fluctuations from each hairpin structure modelled are used as input for a solver of the acoustic diffraction at the trailing edge. The resulting acoustic field is compared against

the standard incoherent wavenumber assumption to verify whether the latter is responsible for the inaccuracies observed in the prediction of noise from serrated trailing edges at high frequencies. Results indicate that the coherent input in the form of idealized hairpin structures does modify the noise reduction spectrum obtained. The spectrum of the noise reduction from a coherent structure is highly dependent on the size of the hairpin and on the spanwise location with respect to the serration. For hairpins centred with the centre and tip of the serration wedge, it is shown that the scattered acoustic field is weakened, pointing to noise reduction. For structures centred with the serration root, the noise is increased. It is shown that the scattering of the large hairpin structures at the root of the serration causes an increase in noise with respect to the straight trailing edge. The spectrum of noise reduction from the combination of the hairpin structures points to a much lower noise reduction compared to the incoherent hypothesis. The results, when confronted with the evidence of lower measured noise reduction from serrated trailing edges, suggest that the assumption of uncorrelated noise sources can be inaccurate to describe the physics of turbulent scattering of non-straight trailing edges.

#### 5. ACKNOWLEDGMENTS

This study is supported by the SMARTANSWER project (Smart Mitigation of flow-induced Acoustic Radiation and Transmission for reduced Aircraft, surface transport, Workplaces and wind energy noise) which has received funding from the European Union's Horizon 2020 research and innovation program under the Marie Skłodowska-Curie grant agreement No. 722401.

#### 6. REFERENCES

- [1] R. K. Amiet, "Noise due to turbulent flow past a trailing edge," *Journal of Sound and Vibration*, vol. 47, no. 3, pp. 387–393, 1976.
- [2] B. Lyu, M. Azarpeyvand, and S. Sinayoko, "Prediction of noise from serrated trailing edges," *Journal of Fluid Mechanics*, vol. 793, pp. 556–588, 2016.
- [3] L. J. Ayton, "Analytic solution for aerodynamic noise generated by plates with spanwise-varying trailing edges," *Journal of Fluid Mechanics*, vol. 849, no. August, pp. 448–466, 2018.
- [4] B. Lyu and L. J. Ayton, "Serrated leading-edge and

trailing-edge noise prediction models for realistic wavenumber frequency spectra,” no. May, 2019.

- [5] G. Grasso, M. Roger, and S. Moreau, “Effect of sweep angle and of wall-pressure statistics on the free-field directivity of airfoil trailing-edge noise,” *25th AIAA/CEAS Aeroacoustics Conference, 2019*, no. May, pp. 1–16, 2019.
- [6] B. Lyu and L. J. Ayton, “Rapid noise prediction models for serrated leading and trailing edges,” *Journal of Sound and Vibration*, vol. 469, p. 115136, 2020.
- [7] M. Sanjosé, S. Moreau, B. Lyu, and L. J. Ayton, “Analytical, numerical and experimental investigation of trailing-edge noise reduction on a Controlled Diffusion airfoil with serrations,” *25th AIAA/CEAS Aeroacoustics Conference*, no. May, 2019.
- [8] C. Arce León, D. Ragni, S. Pröbsting, F. Scarano, and J. Madsen, “Flow topology and acoustic emissions of trailing edge serrations at incidence,” *Experiments in Fluids*, vol. 57, no. 5, 2016.
- [9] M. Gruber, P. Joseph, and T. Chong, “On the mechanisms of serrated airfoil trailing edge noise reduction,” *17th AIAA/CEAS Aeroacoustics Conference (32nd AIAA Aeroacoustics Conference)*, no. June, pp. 5–8, 2011.
- [10] F. Avallone, W. C. van der Velden, and D. Ragni, “Benefits of curved serrations on broadband trailing-edge noise reduction,” *Journal of Sound and Vibration*, vol. 400, no. April, pp. 167–177, 2017.
- [11] F. Avallone, W. C. van der Velden, D. Ragni, and D. Casalino, “Noise reduction mechanisms of sawtooth and combed-sawtooth trailing-edge serrations,” *Journal of Fluid Mechanics*, vol. 848, no. June, pp. 560–591, 2018.
- [12] B. K. Ahn, W. R. Graham, and S. A. Rizzi, *A structure-based model for turbulent-boundary-layer wall pressures*, vol. 650. Delft University of Technology, 2010.
- [13] D. B. Spalding, “A single formula for the “law of the wall”,” *Journal of Applied Mechanics, Transactions ASME*, vol. 28, no. 3, pp. 455–458, 1960.
- [14] D. Coles, “The law of the wake in the turbulent boundary layer,” *Journal of Fluid Mechanics*, vol. 1, no. 2, pp. 191–226, 1956.
- [15] S. Luesutthiviboon, L. T. Lima Pereira, D. Ragni, F. Avallone, and M. Snellen, “{Aeroacoustic Benchmarking of Trailing-edge Noise from a NACA 63<sub>3</sub>-018 Airfoil with Trailing-edge Serrations},” *AIAA Journal*, 2022.
- [16] M. Howe, “Aerodynamic noise of a serrated trailing edge,” *Journal of Fluids and Structures*, vol. 5, pp. 33–45, jan 1991.
- [17] S. Ghaemi and F. Scarano, “Counter-hairpin vortices in the turbulent wake of a sharp trailing edge,” *Journal of Fluid Mechanics*, vol. 689, pp. 317–356, 2011.
- [18] D. M. Chase, “The character of the turbulent wall pressure spectrum at subconvective wavenumbers and a suggested comprehensive model,” *Journal of Sound and Vibration*, vol. 112, no. 1, pp. 125–147, 1987.
- [19] M. Roger and S. Moreau, “Back-scattering correction and further extensions of Amiet’s trailing-edge noise model. Part 1: Theory,” *Journal of Sound and Vibration*, vol. 286, no. 3, pp. 477–506, 2005.
- [20] G. Grasso, P. Jaiswal, H. Wu, S. Moreau, and M. Roger, “Analytical models of the wall-pressure spectrum under a turbulent boundary layer with adverse pressure gradient,” *Journal of Fluid Mechanics*, vol. 877, no. September, pp. 1007–1062, 2019.
- [21] M. Goody, “Empirical Spectral Model of Surface Pressure Fluctuations,” *AIAA Journal*, vol. 42, no. 9, pp. 1788–1794, 2008.